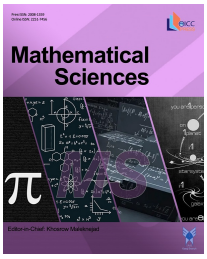

Math. Sci. 2025; 19(4) : 1-18

Mathematical Sciences (MS)

https://doi.org/10.57647/mathsci.2025.1902.18

Green–CAS Wavelet Schemes with Fast Algorithms for Generalized Nonlinear Time–Space Fractional Partial Differential Equations

Muhammad Ismail, Bongsoo Jang*

Department of Mathematical Sciences, Ulsan National Institute of Science and Technology (UNIST), Ulsan 44919, Republic of Korea

***Corresponding author:** bsjang@unist.ac.kr

Original Research

Received:
02 October 2025

Revised:
17 November 2025

Accepted:
20 December 2025

Published online:
30 December 2025

Abstract:

This study aims to acquire numerical schemes to detect the numerical solutions of fractional partial differential equations of arbitrary order, subject to prescribed initial and boundary conditions. This novel approach, referred to as the Green-CAS technique, integrates Green's function with CAS wavelets to construct an efficient and systematic computational framework. The present approach is not only simple and easy to implement due to the Green function, but it also eliminates the need for operational matrices for boundary conditions. To further enhance computational efficiency, a fast algorithm is coupled with the Green-CAS wavelets, enabling effective handling of fractional partial differential equations. While tackling the nonlinear fractional partial differential equation of arbitrary order, the Picard iterative method is employed to transform the equation into a sequence of linear problems, which are then solved using the proposed techniques. Moreover, the order of convergence for two parameters has also been demonstrated in the convergence analysis, which further strengthens the effectiveness of the proposed technique. To show the validity and accuracy of the recommended techniques, the acquired outcomes are compared with the conventional CAS wavelets and various other renowned techniques. In addition, the results of various applications are presented in the form of graphics and tables, which elaborate on the effectiveness and correctness of the discussed method.

Keywords: Caputo derivative; Collocation points; Green-CAS method; Fast algorithm; Picard technique; Fractional partial differential equations (FPDEs)

Cite this article: Ismail M., Jang B. Green–CAS Wavelet Schemes with Fast Algorithms for Generalized Nonlinear Time–Space Fractional Partial Differential Equations Math. Sci 2025; *19*(4) : 1-18 https://doi.org/10.57647/mathsci.2025.1902.18

1. Introduction

In the current era, there is a significant interest among numerous researchers in the pursuit of reputable and competent numerical techniques. This interest arises from the unavailability of exact solutions for differential equations of arbitrary order. To address this challenge, various robust methodologies have been developed. For instance, Lee et al. [1] proposed a novel numerical method for solving nonlinear fractional-order differential equations, demonstrating its applicability across several complex systems. Masti and Sayevand [2] introduced a hybrid collocation-Galerkin scheme utilizing fractional B-spline basis functions to tackle stochastic fractional integro-differential equations. In another advancement, Sivalingam et al. [3] developed an improved L1-type predictor–corrector method tailored to generalized Caputo-type fractional differential equations, enabling accurate temporal discretization and enhanced stability. Zhang et al. [4] presented a high-order spatial scheme for FPDEs that achieves sixth-order accuracy, contributing significantly to the precision of spatial approximations. Ghoreyshi et al. [5] proposed a finite block method for nonlinear time-fractional partial integro-differential equations, providing rigorous stability and convergence analysis along with promising numerical results. Furthermore, Lee et al. [6] developed a high-order, fast computational scheme tailored for Caputo–Fabrizio fractional differential equations characterized by non-singular kernels.

The primary motivation behind this study is to develop a reliable and efficient numerical method for solving FPDEs, which commonly arise in various physical and engineering applications. In particular, we address a generalized class of nonlinear FPDEs incorporating both time and space fractional derivatives, given by

$$\frac{\partial^\alpha u(x,t)}{\partial t^\alpha} + v(x)\frac{\partial^\beta u(x,t)}{\partial x^\beta} + w(x)u(x,t)\frac{\partial^\gamma u(x,t)}{\partial x^\gamma} + y(x)u^p(x,t) = f(x,t), \tag{1}$$

along with the prescribed initial and boundary conditions

$$u(a,t) = u_a(t), \quad u(b,t) = u_b(t),$$
$$(i) \quad u(x,c) = u_c(x), \quad u(x,d) = u_d(x)$$
or
$$(ii) \quad u(x,c) = u_c(x), \quad \left.\frac{\partial u(x,t)}{\partial t}\right|_{t=c} = u_d(x),$$

where $1 < \alpha \le 2$, $1 < \beta \le 2$, $0 < \gamma \le 1$ and $p \ge 1$. In addition to the generalized form presented above, this study also investigates the numerical solution of the prominent fractional model, the nonlinear generalized Burgers-Fisher equation. This equation is widely recognized for its applicability in modeling real-world phenomena involving anomalous transport and nonlinear dynamics. The Burgers-Fisher equation in particular holds significant relevance across various scientific and engineering disciplines, including applied mathematics, physics, gas dynamics, traffic flow modeling, and financial mathematics. Its importance stems from its ability to simultaneously represent convective transport, nonlinear diffusion, and reactive processes. Additionally, the time-fractional Burgers–Fisher equation effectively models the interaction of convection, diffusion, and reaction processes, as demonstrated using the fractional reduced differential transform method [7].

Consider the generalized Burgers-Fisher equation

$$\frac{\partial u(x,t)}{\partial t} - \frac{\partial^2 u(x,t)}{\partial x^2} + au(x,t)^\eta \frac{\partial u(x,t)}{\partial x} + bu(x,t)\Big(u(x,t)^\eta - 1\Big) = 0, \quad 0 \le x \le 1, \ t \ge 0, \tag{2}$$

with the initial and boundary conditions

$$u(x,0) = \left(\frac{1}{2} - \frac{1}{2}\tanh\left(\frac{a\eta}{2(1+\eta)}x\right)\right)^\eta,$$

$$u(0,t) = \left(\tfrac{1}{2} - \tfrac{1}{2}\tanh\left(\tfrac{a\eta}{2(1+\eta)}\left[\left(-\tfrac{a^2+b(1+\eta^2)}{a(1+\eta)}\right)t\right]\right)\right)^\eta,$$
$$u(1,t) = \left(\tfrac{1}{2} - \tfrac{1}{2}\tanh\left(\tfrac{a\eta}{2(1+\eta)}\left[\left(1-\tfrac{a^2+b(1+\eta^2)}{a(1+\eta)}\right)t\right]\right)\right)^\eta.$$

Chen and Zhang in [8] have provided the exact solution for equation (2), which is represented as $u(x,t) = \left(\frac{1}{2} - \frac{1}{2}\tanh\left(\frac{a\eta}{2(1+\eta)}\left[\left(x - \frac{a^2+b(1+\eta)^2}{a(1+\eta)}\right)t\right]\right)\right)^\eta$. For $a \neq 0$, $b = 0$, the generalized Burgers–Fisher equation (2) reduces to the classical Burgers equation, whereas for $a = 0$, $b \neq 0$, it simplifies to the Fisher equation with a fractional temporal derivative [9, 10]. Mesgarani et al. [11] proposed a high-accuracy numerical scheme that combines shifted Chebyshev collocation with compact finite difference methods for solving the time-fractional nonlinear Burgers-Fisher equations, along with rigorous error analysis confirming the method's reliability. Similarly, Aghazadeh [12] proposed a Chebyshev wavelet-based scheme for the generalized time-fractional Burgers–Fisher equation, while Iagar et al. [13] explored its traveling wave solutions, offering analytical insights into nonlinear wave behavior. Various other established numerical techniques have been applied to the Burgers-Fisher equation, including wavelet-based methods [14], iterative solvers [15], and finite difference approaches [16]. For the generalized form (2), the Homotopy Perturbation Method (HPM) has been employed by Rashidi et al. [17]. More recently, modified Laguerre matrix formulations [18] and fourth-order B-spline collocation techniques [19] have been developed to further enhance the accuracy and stability of numerical solutions.

In the recent past, various numerical techniques have been developed with the help of wavelets due to their comprehensive and simple applicabilities. Besides these methods, wavelets have different interesting properties like the capability to demonstrate the functions in various resolution levels and also help to detect singularities that improve the accuracy. A comprehensive list of previous work can be seen in [20]. Additionally, different classes of wavelets have been found in various numerical schemes. For example, B-spline wavelets [21] are employed for the numerical solutions of time-fractional Schrödinger equations. Likewise, Legendre wavelets [22], Haar wavelets [23], Daubechies wavelets [24], and Chebyshev wavelets [25] are used in a wide range of applications. Wavelet-based techniques have also been effectively applied to integral transforms, including Hankel and Fourier–Bessel transforms [26, 27], supported by foundational work on hypergeometric orthogonal polynomials [28] and recent advances in Hankel-transform wavelet frameworks [29]. Several researchers have investigated the application of CAS wavelets as a valuable tool in the numerical approximation of fractional differential and integral equations. Notably, Yousefi and Banifatemi [30] demonstrated their effectiveness in solving linear integral equations, establishing a foundational application of the method. Subsequently, Taher et al. [31] extended the use of CAS wavelets to optimal control systems with time-dependent coefficients, offering a reliable and accurate framework for modeling and analyzing control dynamics. Barzkar et al. [32] further advanced this approach by employing CAS wavelets to develop a numerical scheme for Fredholm–Hammerstein integral equations of the second kind, emphasizing their applicability to nonlinear formulations. Similarly, Mingxu Yi et al. [33] applied CAS wavelets to fractional integro-differential equations of the Bratu type, demonstrating their robustness in capturing the behavior of nonlinear fractional systems.

A method introduced in [34] is extended in this study

https://doi.org/10.57647/mathsci.2025.1902.18

to address FPDEs by incorporating the two-dimensional CAS wavelets and the Green function, called the Green-CAS method. To further improve computational performance and productivity, a fast algorithm is integrated with the Green-CAS framework, resulting in the fast Green-CAS method for the numerical solution of FPDEs. The proposed Fast Green-CAS scheme is specifically designed for time-fractional orders $\alpha \in (0,1)$, where the fast algorithm efficiently approximates the Caputo derivative. These techniques are applied to both linear and nonlinear FPDEs, offering a flexible and effective computational approach. The primary advantages of the proposed Green-CAS and fast Green-CAS techniques are summarized as follows

- Green-CAS technique completely vanishes the operational matrices of integration for boundary value problems.
- Efficiency and accuracy of the Green-CAS method are more better than the conventional CAS wavelet operational methods and various other techniques in the literature.
- The implementation of the fast Green-CAS method for FPDEs is simple and straightforward.
- The fast Green-CAS provides more efficient and productive results compared to Green-CAS.
- The Picard iterative technique, together with the proposed numerical methods, is employed to address the nonlinear problems.
- Order of convergence of two parameters has been investigated and explained in the context of error analysis to enhance the effectiveness of the discussed techniques.

The effectiveness of the Green-CAS and fast Green-CAS techniques is demonstrated through a series of benchmark examples. Numerical results, presented in both graphical and tabular formats, confirm the accuracy and efficiency of the proposed methods. Moreover, comparative analysis with previously established techniques further substantiates the superiority of the presented approaches in solving fractional differential systems.

The sketch of this article is manifested as follows: The second section includes a few essential preliminaries that provide a foundation for our upcoming studies. Sub-part 2.1 comprises CAS wavelets and function approximation that are the basic parts of this work. Section 3.1 explores the Green-CAS method and its implementation procedure for FPDEs. While the procedure of combining the fast algorithm with Green-CAS wavelets is detailed in Subsection 3.2 for FPDEs. Section 4 explains the order of convergence of the suggested technique. The efficiency and accuracy of the Green-CAS and the fast Green-CAS are demonstrated in Section 5, which focuses on the discussion of results from various numerical applications, including a comparison of these outcomes with previous studies to assess the effectiveness of the proposed methods. Also, the subsection 5.2 addresses the application of the Picard method in conjunction with the proposed methods for solving nonlinear problems. Finally, the discussion and concluding remarks are presented in the last section.

2. Preliminaries

The fundamental concept and basic definitions of fractional calculus and CAS wavelets are displayed in this section. These introductory verities help us in the forthcoming sections.

Definition 2.1 *[35, 36] Let $u(x,t) \in C^n([0,1]\times[0,1])$, and let $\alpha \in \mathbb{R}^+$ denote the order of the derivative. The partial Caputo fractional derivative of $u(x,t)$ with respect to the spatial variable x is defined as*

$$\frac{\partial^\alpha u(x,t)}{\partial x^\alpha} = \begin{cases} \mathcal{I}_x^{m-\alpha} \frac{\partial^m u(x,t)}{\partial x^m}, & \alpha \in (m-1, m], \\ \frac{\partial^m u(x,t)}{\partial x^m}, & \alpha = m \in \mathbb{N}. \end{cases}$$

Here, m is defined as the ceiling of α, and $\mathcal{I}_x^{n-\alpha}$ represents the Riemann-Liouville fractional integral operator of order $m-\alpha$. The Riemann-Liouville fractional integral of a function $u(x,t)$ of order $\beta \geq 0$ is given by

$$\mathcal{I}_x^\beta u(x,t) = \begin{cases} \frac{1}{\Gamma(\beta)} \int_a^x (x-\eta)^{\beta-1} u(\eta,t) d\eta, & \beta > 0, \\ u(x,t), & \beta = 0. \end{cases}$$

We present several essential properties of fractional integral and differential operators, as outlined in [35]

- $\mathcal{I}_x^\alpha \mathcal{I}_x^\beta u(x,t) = \mathcal{I}_x^\beta \mathcal{I}_x^\alpha u(x,t) = \mathcal{I}_x^{\alpha+\beta} u(x,t)$.
- $\mathcal{I}_x^\alpha \frac{\partial^\alpha u(x,t)}{\partial x^\alpha} = u(x,t) - \sum_{i=0}^{n-1} \frac{x^i}{\Gamma(i+1)} \frac{\partial^i u(x,t)|_{x=0}}{\partial x^i}, \quad \alpha \in (n-1, n]$.
- $\frac{\partial^\alpha u(x,t)}{\partial x^\alpha} \mathcal{I}_x^\beta u(x,t) = \mathcal{I}_x^{\beta-\alpha} u(x,t), \quad \alpha < \beta$.
- $\frac{\partial^\alpha}{\partial x^\alpha} x^\mu = \frac{\Gamma(\mu+1)}{\Gamma(\mu-\alpha+1)} x^{\mu-\alpha}, \quad \text{for } \alpha,\ \mu \in \mathbb{R}^+$.

2.1 CAS wavelets and function approximations

Wavelets gained significant attention in applied mathematics and related fields beginning in the 1980s, leading to widespread applications across science and engineering. A wavelet family is generated through translation and dilation of a fundamental function known as the mother wavelet, which is defined as

$$\psi_{a,b}(x) = |a|^{-\frac{1}{2}} \psi\left(\frac{x-b}{a}\right), \quad a, b \in \mathbb{R},\ a \neq 0.$$

When $|a| < 1$, the wavelet $\psi_{a,b}(x)$ is compressed in the time domain and corresponds to higher frequencies. In contrast, for $|a| > 1$, the wavelet becomes stretched, capturing lower frequency components. By discretizing the parameters as $a = 2^{-j}$ and $b = 2^{-j}k$ with $j, k \in \mathbb{Z}$, we obtain a countable set of discrete wavelets defined by

$$\psi_{j,k}(x) = 2^{\frac{j}{2}} \psi(2^j x - k).$$

These wavelets, $\psi_{j,k}(x)$, form a complete orthonormal basis for $L^2(\mathbb{R})$, enabling multiresolution analysis and

https://doi.org/10.57647/mathsci.2025.1902.18

efficient function representation [30, 37]. A notable class within this framework is the orthonormal CAS (Cosine and Sine) wavelets, defined over the compact interval $[0, 1]$ as follows [30]

$$\psi_{n,m}(x) = \begin{cases} 2^{\frac{k}{2}} \mathrm{CAS}_m(2^k x - n + 1), & x \in \left[\frac{n-1}{2^k}, \frac{n}{2^k}\right], \\ 0, & \text{otherwise}, \end{cases}$$

where $CAS_m(x) = \cos(2m\pi x) + \sin(2m\pi x)$. The parameter $n = 0,\ 1,\ 2,\ 3,\ \cdots,\ 2^k - 1$ illustrate the translation, while k is a non-negative integer representing the resolution level, and $m \in \mathbb{Z}$. Also, the CAS wavelets possess compact support, which is defined as

$$\mathrm{supp}(\psi_{n,m}(x)) = \overline{\{x : \psi_{n,m}(x) \neq 0\}} = \left[\frac{n-1}{2^k}, \frac{n}{2^k}\right].$$

Function approximations

A function $u(x) \in L^2[0, 1)$ can be approximated using the CAS wavelet basis in the form of an infinite series expansion

$$u(x) = \sum_{n=0}^{\infty} \sum_{m \in \mathbb{Z}} c_{nm} \psi_{n,m}(x), \tag{3}$$

where the wavelet coefficients c_{nm} are defined as $c_{nm} = \langle u(x), \psi_{n,m}(x) \rangle = \int_0^1 u(x)\psi_{n,m}(x)dx$. To facilitate numerical implementation, the infinite series in Equation (3) is truncated as follows

$$u(x) \approx \sum_{n=0}^{2^k-1} \sum_{m=-M}^{M} c_{nm} \psi_{n,m}(x) = C^T \Psi(x), \tag{4}$$

where C and Ψ are column vectors of dimension $2^k(2M+1)$, defined respectively by

$$\begin{aligned} C = [&c_{0,-M}, c_{0,-M+1}, \ldots, c_{0,M}, c_{1,-M}, c_{1,-M+1}, \ldots, \\ &c_{1,M}, \ldots, c_{2^k-1,-M}, c_{2^k-1,-M+1}, \ldots, c_{2^k-1,M}]^T, \\ \Psi(x) = [&\psi_{0,-M}(x), \psi_{0,-M+1}(x), \ldots, \psi_{0,M}(x), \\ &\psi_{1,-M}(x), \psi_{1,-M+1}(x), \ldots, \psi_{1,M}(x), \ldots, \\ &\psi_{2^k-1,-M}(x), \psi_{2^k-1,-M+1}(x), \ldots, \psi_{2^k-1,M}(x)]^T. \end{aligned}$$

The collocation points for evaluating the wavelet basis are chosen as $x_i = \frac{2i-1}{2\hat{m}}$, for $i = 1, 2, \ldots, \hat{m}$. At these points, the CAS wavelet matrix $\Psi_{\hat{m}\times\hat{m}}$ is constructed as

$$\Psi_{\hat{m}\times\hat{m}} = \left[\Psi\left(\frac{1}{2\hat{m}}\right), \Psi\left(\frac{3}{2\hat{m}}\right), \ldots, \Psi\left(\frac{2\hat{m}-1}{2\hat{m}}\right)\right].$$

A function of two variables $u(x, t) \in L_2\Big([0, 1] \times [0, 1]\Big)$, can be approximated by a two-dimensional CAS wavelet expansion as

$$\begin{aligned} u(x,t) &= \sum_{n=0}^{\infty} \sum_{m \in \mathbb{Z}} \sum_{i=0}^{\infty} \sum_{j \in \mathbb{Z}} \psi_{n,m}(x) c_{nm,ij} \psi_{i,j}(t) \\ &\approx \sum_{n=0}^{2^k-1} \sum_{m=-M}^{M} \sum_{i=0}^{2^{k'}-1} \sum_{j=-M'}^{M'} \psi_{n,m}(x) c_{nm,ij} \psi_{i,j}(t) \\ &= \Psi(x)^T C \Psi(t). \end{aligned}$$

CAS wavelets operational matrix

For simplicity, the truncated CAS wavelet expansion in Equation (4) can be written as

$$u(x) \approx \sum_{i=1}^{\hat{m}} c_i \psi_i(x) = C^T \Psi(x),$$

where the index i is defined by $i = M(2n+1)+(m+n+1)$, and $\hat{m} = 2^k(2M + 1)$ represents the total number of wavelet basis functions. Any function $u(x) \in L^2[0, 1)$ can also be approximated using block-pulse functions, as given in [38]

$$u(x) \approx \sum_{i=1}^{\hat{m}} a_i b_i(x) = A^T \mathbf{B}(x),$$

where a_i are the coefficients and $b_i(x)$ are the block-pulse basis functions. The vector $\mathbf{B}(x)$ contains all block-pulse functions defined on the interval. Accordingly, the CAS wavelet vector $\Psi(x)$ can be expanded in terms of the block-pulse basis as

$$\Psi(x) = \Psi_{\hat{m}\times\hat{m}} \mathbf{B}(x),$$

where $\Psi_{\hat{m}\times\hat{m}}$ is the CAS wavelet matrix evaluated at selected collocation points. The fractional integral operator applied to the block-pulse basis is defined by

$$\left(\mathcal{I}_x^{\alpha} \mathbf{B}\right)(x) = K^{\alpha}_{\hat{m}\times\hat{m}} \mathbf{B}(x), \tag{5}$$

where $K^{\alpha}_{\hat{m}\times\hat{m}}$ is detailed in [38, 39], with $P^{\alpha}_{\hat{m}\times\hat{m}} = \Psi_{\hat{m}\times\hat{m}} K^{\alpha} \left[\Psi_{\hat{m}\times\hat{m}}\right]^{-1}$.

3. Green-CAS and fast Green-CAS techniques for the numerical solution of FPDEs

In this section, the Green-CAS and fast Green-CAS techniques are introduced for the numerical solution of FPDEs, considering both initial and boundary conditions. Furthermore, the detailed numerical procedures for implementing each approach are outlined, aiming to obtain accurate and efficient approximations to the solution.

3.1 Green-CAS method

The fractional Green's function, as introduced by Miller and Ross [40], is applicable to FDEs involving derivatives of order $k\alpha$, where k is a positive integer. Based on this formulation, we propose a novel numerical methodology, termed the Green-CAS technique, for solving both linear and nonlinear FPDEs. A significant advantage of the proposed approach lies in its ability to eliminate the use of operational matrices for enforcing boundary conditions, which have traditionally been approximated using block-pulse functions in previous studies. This feature not only simplifies the implementation but also improves computational efficiency. Numerical results demonstrate that the Green-CAS method yields enhanced accuracy and performance in comparison to conventional operational wavelet methods and several other established techniques reported in the literature.

https://doi.org/10.57647/mathsci.2025.1902.18

3.1.1 Mathematical framework of the Green-CAS method

In this subsection, we present the Green-CAS method for computing approximate numerical solutions to linear FPDEs, subject to initial and boundary conditions. We consider the general form of time-space FPDE given by

$$\frac{\partial^\alpha u(x,t)}{\partial t^\alpha} + v(x)\frac{\partial^\beta u(x,t)}{\partial x^\beta} + w(x)\frac{\partial^\gamma u(x,t)}{\partial x^\gamma} + y(x)u(x,t) = f(x,t),\ 1<\alpha,\beta\le 2,\ 0<\gamma\le 1, \quad (6)$$

along with the boundary conditions

$$u(a,t) = u_a(t), \quad u(b,t) = u_b(t), \quad (7)$$

and initial conditions, specified either as

$$(i)\quad u(x,c) = u_c(x), \quad u(x,d) = u_d(x)$$

or

$$(ii)\quad u(x,c) = u_c(x), \quad \left.\frac{\partial u(x,t)}{\partial t}\right|_{t=c} = u_d(x), \quad (8)$$

where $a \le x \le b$, and $0 \le c \le t \le d$. To approximate the highest-order spatial derivative in (6), we express it using a CAS wavelet expansion as follows

$$\frac{\partial^\beta u(x,t)}{\partial x^\beta} \approx \Psi^T(x) C \Psi(t). \quad (9)$$

Applying the Riemann–Liouville integral of order β with respect to x on both sides of (9), we obtain

$$u(x,t) \approx \mathcal{I}_x^\beta \Psi^T(x) C\Psi(t) + x\Phi_1(t) + \Phi_2(t). \quad (10)$$

By incorporating the Dirichlet boundary conditions from (7), we can rewrite (10) in the form

$$\begin{aligned} u(x,t) &\approx \mathcal{I}_x^\beta \Psi^T(x) C\Psi(t) \\ &\quad + \frac{x-a}{a-b}\left(\mathcal{I}_{a,b}^\beta \Psi^T(b) C\Psi(t)\right) \\ &\quad + \frac{x-a}{a-b}\Big(u_a(t) - u_b(t)\Big) + u_a(t) \\ &= \left(\int_a^b G_1(x,\eta)\Psi^T(\eta)\,d\eta\right) C\Psi(t) \\ &\quad + \frac{x-a}{a-b}\Big(u_a(t) - u_b(t)\Big) + u_a(t), \end{aligned} \quad (11)$$

where

$$G_1(x,\eta) = \begin{cases} \dfrac{1}{\Gamma(\beta)}\left((x-\eta)^{\beta-1} + \dfrac{x-a}{a-b}(b-\eta)^{\beta-1}\right), & a \le \eta < x, \\ \dfrac{x-a}{(a-b)\Gamma(\beta)}(b-\eta)^{\beta-1}, & x \le \eta \le b. \end{cases} \quad (12)$$

Here $G_1(x,\eta)$ is called the Green's function. The graph for the function $G_1(x,\eta)$ is shown in [34]. To proceed with the numerical implementation, we approximate the Green's function using CAS wavelet expansion, as follows

$$G_1(x,\eta) \approx \Psi^T(x)\hat{G}_1\Psi(\eta).$$

Utilizing the orthogonality of the CAS wavelet sequence $\psi_{n,m}(t)$ over the interval $[a,b]$, which gives

$$\int_a^b \sum_{n=0}^{2^k-1}\sum_{m=-M}^{M} \psi_{n,m}(\eta)[\psi_{n,m}(\eta)]^T d\eta = \int_a^b \Psi(\eta)\Psi^T(\eta)d\eta = \mathbb{I}_{\hat{m}\times\hat{m}},$$

where $\mathbb{I}_{\hat{m}\times\hat{m}}$ represents the identity matrix. As a result, equation (11) becomes

$$u(x,t) \approx \Psi^T(x)\hat{G}_1 C\Psi(t) + \frac{x-a}{a-b}\Big(u_a(t) - u_b(t)\Big) + u_a(t). \quad (13)$$

Now applying the fractional derivative of order γ with respect to x to equation (11), we obtain

$$\begin{aligned} \frac{\partial^\gamma u(x,t)}{\partial x^\gamma} &\approx \mathcal{I}_x^{\beta-\gamma}\Psi^T(x)C\Psi(t) \\ &\quad + \frac{x^{1-\gamma}}{(a-b)\Gamma(2-\gamma)}\left(\mathcal{I}_{a,b}^\beta \Psi^T(b)C\Psi(t)\right) \\ &\quad + \frac{x^{1-\gamma}}{(a-b)\Gamma(2-\gamma)}\Big(u_a(t) - u_b(t)\Big) \\ &= \left(\int_a^b G_2(x,\eta)\Psi^T(\eta)\,d\eta\right) C\Psi(t) \\ &\quad + \frac{x^{1-\gamma}}{(a-b)\Gamma(2-\gamma)}\Big(u_a(t) - u_b(t)\Big), \end{aligned} \quad (14)$$

where

$$G_2(x,\eta) = \begin{cases} \frac{1}{\Gamma(\beta-\gamma)}(x-\eta)^{\beta-\gamma-1} + \frac{x^{1-\gamma}}{(a-b)\Gamma(2-\gamma)\Gamma(\beta)}(b-\eta)^{\beta-1}, & \text{if } a \le \eta < x, \\ \frac{x^{1-\gamma}}{(a-b)\Gamma(2-\gamma)\Gamma(\beta)}(b-\eta)^{\beta-1}, & \text{if } x \le \eta \le b. \end{cases}$$

Similarly, the Green function $G_2(x,\eta)$ can be approximated using two-dimensional CAS wavelets. By exploiting the orthogonality property of these wavelets, equation (14) is reformulated as follows

$$\begin{aligned} \frac{\partial^\gamma u(x,t)}{\partial x^\gamma} &\approx \Psi^T(x)\hat{G}_2 C\Psi(t) \\ &\quad + \frac{x^{1-\gamma}}{(a-b)\Gamma(2-\gamma)}\Big(u_a(t) - u_b(t)\Big). \end{aligned} \quad (15)$$

Substituting equations (9), (13), and (15) into (6), followed by a rearrangement, we obtain

$$\begin{aligned} \frac{\partial^\alpha u(x,t)}{\partial t^\alpha} &\approx -v(x)\Psi^T(x)C\Psi(t) \\ &\quad - w(x)\Psi^T(x)\hat{G}_2 C\Psi(t) \\ &\quad - y(x)\Psi^T(x)\hat{G}_1 C\Psi(t) + \Psi^T(x)R\Psi(t), \end{aligned} \quad (16)$$

where the function $r(x,t)$ is given as follows, with its approximation by the CAS wavelet expansion

$$\begin{aligned} r(x,t) &= -w(x)\frac{x^{1-\gamma}}{(a-b)\Gamma(2-\gamma)}\Big(u_a(t) - u_b(t)\Big) \\ &\quad - y(x)\frac{x-a}{a-b}\Big(u_a(t) - u_b(t)\Big) \\ &\quad + y(x)u_a(t) + f(x,t) \\ &\approx \Psi^T(x)R\Psi(t). \end{aligned}$$

https://doi.org/10.57647/mathsci.2025.1902.18

Applying the fractional integral operator of order α with respect to t to equation (16) yields an alternative representation for the solution $u(x,t)$. Therefore, we have

$$\begin{aligned} u(x,t) \approx & \Big\{\Big[- v(x)\Psi^T(x) - w(x)\Psi^T(x)\hat{G}_2 \\ & -y(x)\Psi^T(x)\hat{G}_1\Big]C + \Psi^T(x)R\Big\}\mathcal{I}_t^{\alpha}\Psi(t) \\ & +t\theta_1(x) + \theta_2(x). \end{aligned} \tag{17}$$

The functions $\theta_1(x)$ and $\theta_2(x)$ are determined based on the form of the initial conditions provided in equation (8). First we consider the boundary conditions as specified in (8)(i), the equation (17) simplifies to

$$\begin{aligned} u(x,t) \approx & \big\{\big[-v(x)\Psi^T(x) - w(x)\Psi^T(x)\hat{G}_2 \\ & -y(x)\Psi^T(x)\hat{G}_1\big]C + \Psi^T(x)R\big\} \\ & \times \int_c^d G_3(t,\eta)\Psi(\eta)\,d\eta \\ & + \frac{t-c}{c-d}\Big(u_c(x) - u_d(x)\Big) + u_c(x), \end{aligned} \tag{18}$$

where

$$G_3(t,\eta) = \begin{cases} \frac{1}{\Gamma(\alpha)}\left((t-\eta)^{\alpha-1}\right. & \text{if } c \le \eta < t, \\ \left. + \frac{t-c}{c-d}(d-\eta)^{\alpha-1}\right), & \\ \frac{t-c}{(c-d)\Gamma(\alpha)}(d-\eta)^{\alpha-1}, & \text{if } t \le \eta \le d. \end{cases}$$

Again using the approximation of Green function $G_3(t,\eta)$ by using CAS wavelets and applying the orthogonality property, equation (18) becomes

$$\begin{aligned} u(x,t) \approx & \big\{\big[-v(x)\Psi^T(x) - w(x)\Psi^T(x)\hat{G}_2 \\ & -y(x)\Psi^T(x)\hat{G}_1\big]C + \Psi^T(x)R\big\}\hat{G}_3\Psi(t) \\ & + \frac{t-c}{c-d}\Big(u_c(x) - u_d(x)\Big) + u_c(x). \end{aligned} \tag{19}$$

Now, considering the second type of initial condition defined in (8)(ii), equation (17) is rewritten as

$$\begin{aligned} u(x,t) \approx & \big\{\big[-v(x)\Psi^T(x) - w(x)\Psi^T(x)\hat{G}_2 \\ & -y(x)\Psi^T(x)\hat{G}_1\big]C + \Psi^T(x)R\big\}P^{\alpha} \\ & +(t-c)u_d(x) + u_c(x), \end{aligned} \tag{20}$$

where P^{α} is the operation matrix given in equation (5). Equating the right hand sides of equations (13) and (19), followed by a rearrangement, leads to the following expression

$$\begin{aligned} & \Psi^T(x)\hat{G}_1C\Psi(t) + \big\{\big[v(x)\Psi^T(x) + w(x)\Psi^T(x)\hat{G}_2 \\ & +y(x)\Psi^T(x)\hat{G}_1\big]C\big\}\hat{G}_3\Psi(t) = \Psi^T(x)R\hat{G}_3\Psi(t) \\ & +h(x,t), \end{aligned} \tag{21}$$

where $h(x,t) = -\frac{x-a}{a-b}\big(u_a(t) - u_b(t)\big) + \frac{t-c}{c-d}\big(u_c(x) - u_d(x)\big) - u_a(t) + u_c(x)$. Evaluating equation (21) at the collocation points $x_i = \frac{2i-1}{2\hat{m}}$ and $t_j = \frac{2j-1}{2m'}$, where $i = 1,2,\ldots,\hat{m}$, $j = 1,2,\ldots,m'$, yields the algebraic system

$$\begin{aligned} & \Psi^T_{\hat{m}\times\hat{m}}\hat{G}_1C\Psi_{m'\times m'} + \{A_{\hat{m}\times\hat{m}}C\}\,\hat{G}_3\Psi_{m'\times m'} \\ & = \Psi^T_{\hat{m}\times\hat{m}}R\hat{G}_3\Psi_{m'\times m'} + H, \end{aligned}$$

where $A_{\hat{m}\times\hat{m}} = \left[\mathbb{V}\Psi^T_{\hat{m}\times\hat{m}} + \mathbb{W}\Psi^T_{\hat{m}\times\hat{m}}\hat{G}_2 + \mathbb{Y}\Psi^T_{\hat{m}\times\hat{m}}\hat{G}_1\right]$. The above equation can be reformulated into the standard Sylvester matrix form as

$$\begin{aligned} & A^{-1}_{\hat{m}\times\hat{m}}\Psi^T_{\hat{m}\times\hat{m}}\hat{G}_1C + C\hat{G}_3 \\ & - A^{-1}_{\hat{m}\times\hat{m}}\left(\Psi^T_{\hat{m}\times\hat{m}}R\hat{G}_3 + H[\Psi_{m'\times m'}]^{-1}\right) = 0. \end{aligned} \tag{22}$$

The matrices $\mathbb{V}$, $\mathbb{W}$, and $\mathbb{Y}$ are defined as diagonal matrices constructed from the evaluation of $v(x)$, $w(x)$, and $y(x)$ at the collocation points

$$\mathbb{V} = \begin{bmatrix} v(x_1) & 0 & \cdots & 0 \\ 0 & v(x_2) & \cdots & 0 \\ \vdots & \vdots & \ddots & \vdots \\ 0 & 0 & \cdots & v(x_{\hat{m}}) \end{bmatrix},$$

$$\mathbb{W} = \begin{bmatrix} w(x_1) & 0 & \cdots & 0 \\ 0 & w(x_2) & \cdots & 0 \\ \vdots & \vdots & \ddots & \vdots \\ 0 & 0 & \cdots & w(x_{\hat{m}}) \end{bmatrix},$$

$$\mathbb{Y} = \begin{bmatrix} y(x_1) & 0 & \cdots & 0 \\ 0 & y(x_2) & \cdots & 0 \\ \vdots & \vdots & \ddots & \vdots \\ 0 & 0 & \cdots & y(x_{\hat{m}}) \end{bmatrix}.$$

Equation (22) represents a Sylvester matrix system. The numerical solution proceeds by solving the system given in (22) to determine the unknown coefficient matrix C. Once obtained, the matrix C is substituted into equation (13) or (19) to get the approximate solution $u(x,t)$.

In addition, for the second type of initial condition specified in (8)(ii), an another algebraic system is derived by combining equations (13) and (20), evaluated at the collocation points is given as follows

$$\Psi^T_{\hat{m}\times\hat{m}}\hat{G}_1C\Psi_{m'\times m'} + A_{\hat{m}\times\hat{m}}CP^{\alpha}_{m'\times m'} = \Psi^T_{\hat{m}\times\hat{m}}RP^{\alpha}_{m'\times m'} + S,$$

which, upon rearrangement, takes the form of a Sylvester-type equation

$$\begin{aligned} & A^{-1}_{\hat{m}\times\hat{m}}\Psi^T_{\hat{m}\times\hat{m}}\hat{G}_1C + CP^{\alpha}_{m'\times m'}\left[\Psi_{m'\times m'}\right]^{-1} \\ & -A^{-1}_{\hat{m}\times\hat{m}}\left(\Psi^T_{\hat{m}\times\hat{m}}RP^{\alpha}_{m'\times m'} + S\right)\left[\Psi_{m'\times m'}\right]^{-1} = 0, \end{aligned} \tag{23}$$

where, S represents the function $s(x,t) = -\frac{x-a}{a-b}\big(u_a(t) - u_b(t)\big) + (t-c)u_d(x) - u_a(t) + u_c(x)$ at the collocation points. Solving equation (23) yields the coefficient matrix C associated with the second initial conditions (8)(ii). This matrix can then be inserted into equation (13) or (20) to obtain the numerical solution.

3.2 Fast Green-CAS wavelet scheme for solving FPDEs

In this section, we combine the fast algorithm with Green-CAS wavelets. This combination proves highly efficient in handling FPDEs. Also, this approach demonstrates swiftness in yielding outcomes. To execute this strategy, we implement a fast algorithm for time derivatives within FPDEs and Green-CAS wavelets for the spatial derivatives.

To evaluate the Caputo fractional derivative of order $0 < \alpha < 1$ over a uniform temporal grid $\{t_n \mid t_n = n\Delta t,\ n = 0, 1, \ldots, N\}$, we consider the following decomposition

$$\begin{aligned}\frac{\partial^\alpha u(t_n)}{\partial t^\alpha} &= \frac{1}{\Gamma(1-\alpha)}\int_0^{t_n}\frac{\partial u(\tau)}{\partial \tau}(t_n-\tau)^{-\alpha}d\tau \\ &= C_l(t_n) + C_h(t_n),\end{aligned}$$

where the integral is split into two parts

$$C_l(t_n) = \frac{1}{\Gamma(1-\alpha)}\int_{t_{n-1}}^{t_n}\frac{\partial u(\tau)}{\partial \tau}(t_n-\tau)^{-\alpha}d\tau,$$
$$C_h(t_n) = \frac{1}{\Gamma(1-\alpha)}\int_0^{t_{n-1}}\frac{\partial u(\tau)}{\partial \tau}(t_n-\tau)^{-\alpha}d\tau.$$

where $C_l(t_n)$ and $C_h(t_n)$ represent the local part and history part, respectively. The local term $C_l(t_n)$ can be approximated using linear interpolation between t_{n-1} and t_n, yielding

$$C_l(t_n) \approx \frac{1}{\Gamma(2-\alpha)}\left[\frac{u(t_n)-u(t_{n-1})}{\Delta t^\alpha}\right].$$

The history term $C_h(t_n)$ is approximated using the sum-of-exponentials (SOE) approach, as described in [41]. The resulting expression is

$$C_h(t_n) \approx \frac{1}{\Gamma(1-\alpha)}\left[\frac{u(t_{n-1})}{\Delta t^\alpha} - \frac{u(t_0)}{t_n^\alpha} - \alpha\sum_{i=1}^{N_{\exp}}\omega_i H_{\text{hist},i}(t_n)\right],$$

where $H_{\text{hist},i}(t_n) = \int_0^{t_{n-1}} e^{-s_i(t_n-\tau)}u(x,\tau)\,d\tau$. The parameters (ω_i, s_i) denote the weights and nodes obtained using the quadrature strategy provided in Algorithm 1 of [**LEE2024**]. Accordingly, the history term $H_{\text{hist},i}(t_n)$, can be written as

$$\begin{aligned}H_{\text{hist},i}(t_n) &\approx e^{-s_i\Delta t}H_{\text{hist},i}(t_{n-1}) \\ &\quad + \frac{e^{-s_i\Delta t}}{s_i^2\Delta t}\Big[(e^{-s_i\Delta t} - 1 + s_i\Delta t)u(t_{n-1}) \\ &\quad + (1 - e^{-s_i\Delta t} - e^{-s_i\Delta t}s_i\Delta t)u(t_{n-2})\Big].\end{aligned}$$

Therefore, the Caputo fractional derivative of order α with respect to t can be approximated as follows

$$\begin{aligned}\frac{\partial^\alpha u(t_n)}{\partial t^\alpha} &\approx \frac{u(t_n)}{\Gamma(2-\alpha)\Delta t^\alpha} \\ &\quad + \frac{u(t_{n-1})}{\Delta t^\alpha}\left[\frac{1}{\Gamma(1-\alpha)} - \frac{1}{\Gamma(2-\alpha)}\right] \\ &\quad - \frac{1}{\Gamma(1-\alpha)}\left[\frac{u(t_0)}{t_n^\alpha} + \alpha\sum_{i=1}^{N_{\exp}}\omega_i U_{\text{hist},i}(t_n)\right].\end{aligned} \tag{24}$$

Lemma 3.1 *[41] Suppose $u(t) \in C^2[t_0, t_n]$, and define $R(u(t_n)) = \frac{\partial^\alpha u(t_n)}{\partial t^\alpha} - \frac{\partial^\alpha u^n}{\partial t^\alpha}$, then we can conclude that*

$$\begin{aligned}|R(u(t_n))| &\le \frac{\Delta^{2-\alpha}}{\Gamma(2-\alpha)}\Big(\frac{1-\alpha}{12} + \frac{2^{2-\alpha}}{2-\alpha} \\ &\quad -(1+2^{-\alpha})\Big)\max_{t_0\le t\le t_n}|u''(t)| \\ &\quad + \frac{\alpha\epsilon t_{n-1}}{\Gamma(1-\alpha)}\max_{t_0\le t\le t_n}|u(t)|,\end{aligned}$$

where

$$\begin{aligned}\frac{\partial^\alpha u^n}{\partial t^\alpha} &= \frac{u(t_n)}{\Gamma(2-\alpha)\Delta t^\alpha} \\ &\quad + \frac{u(t_{n-1})}{\Delta t^\alpha}\left[\frac{1}{\Gamma(1-\alpha)} - \frac{1}{\Gamma(2-\alpha)}\right] \\ &\quad - \frac{1}{\Gamma(1-\alpha)}\left[\frac{u(t_0)}{t_n^\alpha} + \alpha\sum_{i=1}^{N_{\exp}}\omega_i U_{hist,i}(t_n)\right].\end{aligned}$$

3.2.1 Merging fast algorithm with Green-CAS wavelet

In this subsection, we introduce an efficient approach referred to as the fast Green-CAS technique for the numerical solution of FPDEs with a time fractional order in the interval $(0, 1)$. Particularly, we consider the following form

$$\begin{aligned}&\frac{\partial^\alpha u(x,t)}{\partial t^\alpha} + v(x)\frac{\partial^\beta u(x,t)}{\partial x^\beta} \\ &+w(x)\frac{\partial^\gamma u(x,t)}{\partial x^\gamma} + y(x)u(x,t) = f(x,t), \\ &0 < \alpha < 1,\ 1 < \beta \le 2, 0 < \gamma \le 1,\end{aligned} \tag{25}$$

along with the initial and boundary conditions

$$\begin{aligned}u(x,c) &= u_c(x), \\ u(a,t) = u_a(t), &\quad u(b,t) = u_b(t).\end{aligned} \tag{26}$$

Since the approximation of the Caputo fractional derivative at the time step t_n as described in equation (24) as

$$\begin{aligned}\frac{\partial^\alpha u(t_n)}{\partial t^\alpha} &\approx \frac{u(t_n)}{\Gamma(2-\alpha)\Delta t^\alpha} \\ &\quad + \frac{u(t_{n-1})}{\Delta t^\alpha}\left[\frac{1}{\Gamma(1-\alpha)} - \frac{1}{\Gamma(2-\alpha)}\right] \\ &\quad - \frac{1}{\Gamma(1-\alpha)}\left[\frac{u(t_0)}{t_n^\alpha} + \alpha\sum_{i=1}^{N_{\exp}}\omega_i U_{\text{hist},i}(t_n)\right].\end{aligned} \tag{27}$$

Substitute equation (27) into equation (25), followed by rearrangement we have

$$\begin{aligned}&\left(\frac{1}{\Gamma(2-\alpha)\Delta t^\alpha} + y(x)\right)u(x,t_n) + v(x)\frac{\partial^\beta u(x,t)}{\partial x^\beta} \\ &+w(x)\frac{\partial^\gamma u(x,t)}{\partial x^\gamma} + y(x)u(x,t) = g(x,t),\end{aligned} \tag{28}$$

where $g(x,t_n) = f(x,t_n) - \frac{u(x,t_{n-1})}{\Delta t^\alpha}\left[\frac{1}{\Gamma(1-\alpha)} - \frac{1}{\Gamma(2-\alpha)}\right] + \frac{1}{\Gamma(1-\alpha)}\left[\frac{u(x,t_0)}{t_n^\alpha} + \alpha\sum_{i=1}^{N_{exp}}\omega_i U_{hist,i}(x,t_n)\right]$. Estimating the

https://doi.org/10.57647/mathsci.2025.1902.18

highest order of the Caputo fractional derivative with order β by employing a truncated series composed as follows

$$\frac{\partial^\beta u(x,t_n)}{\partial x^\beta} \approx [C^n]^T \Psi(x). \tag{29}$$

Now, we apply the appropriate Riemann-Liouville integration technique with respect to the variable x. Following this integration process, we also consider the relevant boundary conditions as specified in (26), and using the approximation of Green function. As a consequence of these steps, we derive the following expression

$$\begin{aligned} u(x,t_n) &\approx [C^n]^T \mathcal{I}_x^\beta \Psi(x) \\ &\quad + [C^n]^T \frac{x-a}{a-b}\left(\mathcal{I}_{a,b}^\beta \Psi(b)\right) \\ &\quad + \frac{x-a}{a-b}\Big(u_a(t)-u_b(t)\Big) + u_a(t) \\ &= [C^n]^T \hat{G}_1^n \Psi(x) \\ &\quad + \frac{x-a}{a-b}\Big(u_a(t)-u_b(t)\Big) + u_a(t). \end{aligned} \tag{30}$$

Similarly, applying the fractional derivative of order γ with respect to x to equation (30), to obtain the approximation of $\frac{\partial^\gamma u(x,t)}{\partial x^\gamma}$, we have

$$\begin{aligned} \frac{\partial^\gamma u(x,t_n)}{\partial x^\gamma} &\approx [C^n]^T \mathcal{I}_x^{\beta-\gamma} \Psi(x) \\ &\quad + [C^n]^T \frac{x^{1-\gamma}}{(a-b)\Gamma(2-\gamma)}\left(\mathcal{I}_{a,b}^\beta \Psi(b)\right) \\ &\quad + \frac{x^{1-\gamma}}{(a-b)\Gamma(2-\gamma)}\Big(u_a(t)-u_b(t)\Big) \\ &= [C^n]^T \hat{G}_2^n \Psi(x) \\ &\quad + \frac{x^{1-\gamma}}{(a-b)\Gamma(2-\gamma)}\Big(u_a(t)-u_b(t)\Big). \end{aligned} \tag{31}$$

In order to find the $[C^n]^T$, it is necessary to substitute equations (29), (30) and (31) into equation (28), and subsequently rearrange the terms. So we will have the following expression

$$\begin{aligned} [C^n]^T \Bigg[\Big(\frac{1}{\Gamma(2-\alpha)\Delta t^\alpha} + y(x)\Big)\hat{G}_1^n \Psi(x) \\ + v(x)\Psi(x) + w(x)\hat{G}_2^n \Psi(x) \Bigg] = [K^n]^T \Psi(x), \end{aligned} \tag{32}$$

where

$$\begin{aligned} k(x,t_n) =& g(x,t_n) - \Big(\frac{1}{\Gamma(2-\alpha)\Delta t^\alpha} + y(x)\Big) \\ &\times \left[\frac{x-a}{a-b}\Big(u_a(t)-u_b(t)\Big) + u_a(t)\right] \\ &- w(x)\frac{x^{1-\gamma}}{(a-b)\Gamma(2-\gamma)}\Big(u_a(t)-u_b(t)\Big) \end{aligned}$$

Therefor equation (32) can be written at the collocation points as

$$\begin{aligned} [C^n]^T \Bigg[\Big(\frac{1}{\Gamma(2-\alpha)\Delta t^\alpha} + \mathbb{Y}\Big)\hat{G}_1^n \Psi_{\hat{m}\times\hat{m}} \\ + \mathbb{V}\Psi_{\hat{m}\times\hat{m}} + \mathbb{W}\hat{G}_2^n \Psi_{\hat{m}\times\hat{m}} \Bigg] = [K^n]^T. \end{aligned} \tag{33}$$

Once $[C^n]^T$ is computed from equation (33), it is substituted back into (30) to compute the numerical solution at the desired time level.

4. Convergence analysis

In this section, we examine the convergence behavior of the proposed technique. We begin by considering the general form of a fractional partial differential equation

$$G\left(x,t,u(x,t),\frac{\partial^\alpha u(x,t)}{\partial x^\alpha},\frac{\partial^\beta u(x,t)}{\partial x^\beta}\right) = 0,$$
$$0 < \alpha \le 1, \quad 1 \le \beta \le 2,$$

where α and β denote the orders of the spatial fractional derivatives. Following the standard approach, the higher-order fractional derivative is approximated using a CAS wavelet expansion as

$$\frac{\partial^\beta u(x,t)}{\partial x^\beta} = \sum_{n=0}^{\infty}\sum_{m\in\mathbb{Z}}\sum_{i=0}^{\infty}\sum_{j\in\mathbb{Z}} \psi_{n,m}(x) c_{nm,ij} \psi_{i,j}(t). \tag{34}$$

Now, by integrating the equation (34) and incorporating boundary conditions, and applying the procedure outlined from equations (10) to (13), the solution can be represented as

$$\begin{aligned} u(x,t) = &\sum_{n=0}^{\infty}\sum_{m\in\mathbb{Z}}\sum_{i=0}^{\infty}\sum_{j\in\mathbb{Z}} \hat{G}_{nm,ij}\psi_{n,m}(x)c_{nm,ij}\psi_{i,j}(t) \\ &+ \frac{x-a}{a-b}\Big(u_a(t)-u_b(t)\Big) + u_a(t). \end{aligned} \tag{35}$$

Here u_a and u_b are the boundary values, and $\hat{G}_{nm,ij}$ are the coefficients associated with the Green's function $G(x,\eta)$, defined in equation (12). The approximation of the Green function by CAS wavelets is given as

$$G(x,\eta) = \sum_{n=0}^{\infty}\sum_{m\in\mathbb{Z}}\sum_{i=0}^{\infty}\sum_{j\in\mathbb{Z}} \psi_{n,m}(x)\hat{G}_{nm,ij}\psi_{i,j}(\eta),$$

where the coefficients are computed as $\hat{G}_{nm,ij} = \langle\langle G(x,\eta),\psi_{n,m}(x)\rangle,\psi_{i,j}(\eta)\rangle$.

Theorem 4.1 *Consider* $f(x,t) = \frac{\partial^\beta u(x,t)}{\partial x^\beta} \in L^2([0,1]\times[0,1])$ *is differentiable, and its partial derivative is bounded on* $([0,1]\times[0,1])$. *That is, there exists* $L > 0$ *such that* $\left|\frac{\partial^2 u(x,t)}{\partial x^2}\right| \le L$ *for all* $(x,t) \in ([0,1]\times[0,1])$. *Then the order of convergence of the Green-CAS wavelet is given by*

$$\begin{aligned} ||u(x,t) - u_{kM}(x,t)||_2 &= ||E_{Mk}||_2 \\ &= O\left(\left(\frac{1}{M+1}\right)\left(\frac{1}{2^k}\right)^{\frac{3}{2}}\right). \end{aligned}$$

Proof. Consider $u_{kM}(x,t)$ denote the truncated Green-CAS approximation of $u(x,t)$ as given in (35). Therefore

$$\begin{aligned} u_{kM}(x,t) = &\sum_{n=0}^{2^k-1}\sum_{m=-M}^{M}\sum_{i=0}^{2^{k'}-1}\sum_{j=-M'}^{M'} \\ &\hat{G}_{nm,ij}\psi_{n,m}(x)c_{nm,ij}\psi_{i,j}(t) \\ &+ \frac{x-a}{a-b}\Big(u_a(t)-u_b(t)\Big) + u_a(t). \end{aligned}$$

https://doi.org/10.57647/mathsci.2025.1902.18

Then, we have

$$|u(x,t)-u_{kM}(x,t)| = \Big|\sum_{n=2^k}^{\infty}\sum_{m=M+1}^{\infty}\sum_{i=2^{k'}}^{\infty}\sum_{j=M'+1}^{\infty} \hat{G}_{nm,ij}\psi_{n,m}(x)c_{nm,ij}\psi_{i,j}(t)\Big|.$$

By expanding the square of the L_2-norm of the error function, we have

$$\begin{aligned}||u(x,t)-u_{kM}(x,t)||^2 &= \Big\|\sum_{n=2^k}^{\infty}\sum_{m=M+1}^{\infty}\sum_{i=2^{k'}}^{\infty}\sum_{j=M'+1}^{\infty} \hat{G}_{nm,ij}\psi_{n,m}(x)c_{nm,ij}\psi_{i,j}(t)\Big\|^2\\ &= \int_0^1\int_0^1\Big|\sum_{n=2^k}^{\infty}\sum_{m=M+1}^{\infty}\sum_{i=2^{k'}}^{\infty}\sum_{j=M'+1}^{\infty} \hat{G}_{nm,ij}\psi_{n,m}(x)c_{nm,ij}\psi_{i,j}(t)\Big|^2 dxdt\\ &\le \sum_{n=2^k}^{\infty}\sum_{m=M+1}^{\infty}\sum_{i=2^{k'}}^{\infty}\sum_{j=M'+1}^{\infty} |\hat{G}_{nm,ij}|^2|c_{nm,ij}|^2\int_0^1|\psi_{n,m}(x)|^2dx\\ &\times\int_0^1|\psi_{i,j}(t)|^2dt. \end{aligned} \tag{36}$$

As $c_{nm,ij}$ and $\hat{G}_{nm,ij}$ are constant functions and since $\int_0^1|\psi_{n,m}(x)|^2dx = 1$ and $\int_0^1|\psi_{i,j}(t)|^2dt = 1$. Therefore, (36) we can be write as

$$||u(x,t)-u_{kM}(x,t)||^2 \le \sum_{n=2^k}^{\infty}\sum_{m=M+1}^{\infty}\sum_{i=2^{k'}}^{\infty}\sum_{j=M'+1}^{\infty} |\hat{G}_{nm,ij}|^2|c_{nm,ij}|^2. \tag{37}$$

Since we know the coefficient $c_{nm,ij}$ can be found as

$$\begin{aligned}c_{nm,ij} &= \langle\langle u(x,t),\psi_{n,m}(x)\rangle,\psi_{j,i}(t)\rangle\\ &= \int_0^1\Big[\int_0^1 u(x,t)\psi_{n,m}(x)dx\Big]\psi_{i,j}(t)dt.\end{aligned}$$

Utilizing the definition of CAS wavelets, we have

$$\begin{aligned}c_{nm,ij} &= 2^{\frac{k}{2}}2^{\frac{k'}{2}}\int_{\frac{i-1}{2^{k'}}}^{\frac{i}{2^{k'}}}\Big[\int_{\frac{n-1}{2^k}}^{\frac{n}{2^k}} u(x,t)\\ &\times CAS_m(2^kx-n+1)dx\Big]CAS_j(2^{k'}t-i+1)dt\\ &= \frac{1}{2^{\frac{k}{2}}2^{\frac{k'}{2}}}\int_0^1\Big[\int_0^1 u\Big(\frac{v+n-1}{2^k},\frac{w+i-1}{2^{k'}}\Big)\\ &\times\Big(\cos(2m\pi v)+\sin(2m\pi v)\Big)dv\Big]\\ &\times\Big(\cos(2m\pi w)+\sin(2m\pi w)\Big)dw.\end{aligned}$$

Applying integration by parts with respect to "v" and then "w", we have

$$\begin{aligned}c_{nm,ij} =& \frac{1}{4mj\pi^2 2^{\frac{3k}{2}}2^{\frac{3k'}{2}}}\int_0^1\int_0^1\frac{\partial^2 u}{\partial v\partial w}\Big(\frac{v+n-1}{2^k},\\ &\frac{w+i-1}{2^{k'}}\Big)\Big(\sin(2m\pi v)-\cos(2m\pi v)\Big)dv\\ &\times\Big(\sin(2m\pi w)-\cos(2m\pi w)\Big)dw.\end{aligned}$$

Since $|\frac{\partial^2 u(x,t)}{\partial x^2}| \le L$ and $\Big|\sin(2m\pi x)-\cos(2m\pi x)\Big| \le 4$, it follows that

$$|c_{mn,ij}|^2 \le \left|\frac{L}{mj\pi^2 2^{\frac{3k}{2}}2^{\frac{3k'}{2}}}\right|^2 \le \left|\frac{L}{mj\pi^2 n^{\frac{3}{2}}i^{\frac{3}{2}}}\right|^2. \tag{38}$$

Since constant $\hat{G}_{nm,ij}$ is defined as $\hat{G}_{nm,ij} = \langle\langle G(x,\eta),\psi_{n,m}(x)\rangle,\psi_{i,j}(\eta)\rangle$. Therefore

$$|\hat{G}_{nm,ij}| \le \big|\langle\langle G(x,\eta),\psi_{n,m}(x)\rangle,\psi_{i,j}(\tau)\rangle\big| = K' < \infty. \tag{39}$$

By substituting equations (38) and (39) into equation (37), we obtain the following expression:

$$\begin{aligned}&\|u(x,t)-u_{kM}(x,t)\|^2\\ &= \sum_{n=2^k}^{\infty}\sum_{m=M+1}^{\infty}\sum_{n=2^{k'}}^{\infty}\sum_{m=M'+1}^{\infty}\left|\frac{K'L}{mj\pi^2 n^{\frac{3}{2}}i^{\frac{3}{2}}}\right|^2\\ &\le \left|\frac{Q}{(M+1)(M'+1)\pi^2(2^k)^{\frac{3}{2}}(2^{k'})^{\frac{3}{2}}}\right|^2.\end{aligned}$$

Hence

$$\begin{aligned}\|E_{Mk}\|_2 &= \|u(x,t)-y^{k,k',M,M'}(x,t)\|_2\\ &= O\left(\left(\frac{1}{M+1}\right)\left(\frac{1}{2^k}\right)^{\frac{3}{2}}\right).\end{aligned} \tag{40}$$

The numerical evaluation of the order of convergence follows the procedure adopted in [42]. Let us consider the constant $\omega = \frac{Q}{(M+1)\pi^2}$, with p treated as a variable in the convergence estimate of equation (40). This leads to the following form

$$F(h)-F(0) = \omega h^p + O(h^l), \quad 0 < p < l,$$

where $F(h)$ denotes the numerical solution corresponding to step size h, and $F(0)$ denotes the exact solution. The value p represents the theoretical order of convergence of the method.

Considering the step sizes h_{i-1} and $h_i = \frac{h_{i-1}}{2}$, with corresponding numerical solutions $F_{i-1} = F(h_{i-1})$ and $F_i = F(h_i)$. The estimated convergence order of the given method is then computed as

$$p = \log\left(\frac{\|F_{i-1}-F(0)\|}{\|F_i-F(0)\|}\right)\Big/\log(2).$$

Furthermore, when the constant is expressed as $\omega = \frac{Q}{\pi^2}\left(\frac{1}{2^k}\right)^{\frac{3}{2}}$, and M is treated as the variable in equation (40), the convergence order with respect to M tends

toward one. This behavior is characterized by

$$\left(\frac{\|E_{M+1}\|_2}{\|E_{M+2}\|_2}\right) = \frac{M+2}{M+1}, \quad \text{for } M = 1,\ 2,\ 3,\ \cdots.$$

Remarks:
According to the convergence analysis of the Green-CAS method discussed in Theorem 4.1, and the fast algorithm presented in Lemma 3.1, we conclude that the fast Green-CAS method as discussed in section 3.2, yields a solution that converges to the exact solution $u(x,t)$ as the parameters $k, M \to \infty$ and the time step $\Delta t \to 0$.

5. Applications

In this section, we present several numerical examples to evaluate the validity and efficiency of the proposed Green-CAS and fast Green-CAS techniques. To further demonstrate the effectiveness of these approaches, a comparative analysis is also conducted against the conventional operational CAS wavelet method and previously reported results in the literature.

5.1 Linear Fractional Problems

Example 5.1 *Assume the time-fractional diffusion equation[43, 44], along with the initial and boundary conditions*

$$\begin{aligned} \frac{\partial^\alpha u(x,t)}{\partial t^\alpha} &= \frac{x^2}{2}\frac{\partial^2 u(x,t)}{\partial x^2}, \qquad 0 < x < 1,\ \ 0 < t \le 1, \\ u(0,t) &= 0, \qquad u(1,t) = \exp(t), \\ u(x,0) &= x^2, \end{aligned} \tag{41}$$

where $0 < \alpha \le 1$. When α is set to 1, the equation (41) has an analytic solution, which is $u(x,t) = x^2\exp(t)$. The numerical solutions can be acquired using the proposed technique detailed in Section 3.1.1. Table 1 presents the absolute errors for $\alpha = 1$, maintaining the same number of steps as given in [43], with $k = 5$ and $M = 5$ in both spatial and temporal directions. The results clearly demonstrate the reliability and improved accuracy of the proposed approach compared to the Sinc–Legendre collocation method (S-LCM) presented in [43], as well as the variational iteration method (VIM) and Adomian decomposition method (ADM) discussed in [44]. Additionally, Table 2 and Figure 1 validate the theoretical order of convergence as described in the error analysis for k and M. Furthermore, to facilitate a comparative analysis between the Green-CAS and the fast Green-CAS methods, we have also solved the equation (5.1) using the fast Green-CAS approach. The corresponding numerical results for both methods are summarized in Table 3. It is evident from the tabulated results that the fast Green-CAS method achieves a substantially reduced computational time compared to the Green-CAS technique. Moreover, the fast Green-CAS wavelet approach exhibits marginally improved accuracy, particularly for larger time step sizes. This computational advantage is further illustrated in Figure 2, where the CPU time required by the fast Green-CAS method is consistently lower than that of the Green-CAS method for increasing time steps.

Example 5.2 *Consider the linear multi-term fractional convection-diffusion equation given by*

$$\frac{\partial^\alpha u(x,t)}{\partial t^\alpha} = a(x)\frac{\partial^\beta u(x,t)}{\partial x^\beta} - b(x)\frac{\partial^\gamma u(x,t)}{\partial x^\gamma} + f(x,t), \tag{42}$$

where $\alpha, \beta \in (1,2]$ and $\gamma \in (0,1)$. The problem is formulated with initial and boundary conditions given by $u(x,0) = u(x,1) = 0$, $u(0,t) = u(1,t) = 0$. Here, the coefficient functions are $a(x) = \Gamma(2\beta+2)\Gamma(5-\alpha-\beta)x^\beta$, $b(x) = \Gamma(3\beta+2-\gamma)\Gamma(5-2\gamma)x^\gamma$ and $f(x,t) = -(x^{3\beta+1} - x^{4-\gamma})(3\pi)^3 t^{3-\alpha}E_{2,4-\alpha}(-(3\pi t)^2) + \Big\{\Gamma(3\beta+2)\big[\Gamma(5-2\gamma) - \Gamma(5-\gamma-\beta)\big]x^{3\beta+1} + \Gamma(5-\gamma)\big[\Gamma(2\beta+2) - \Gamma(3\beta-\gamma+2)\big]x^{4-\gamma}\Big\}\sin(3\pi t)$. This enables us to conventionally verify that the exact solution to equation (42) is

$$u(x,t) = \left(x^{3\beta+1} - x^{4-\gamma}\right)\sin(3\pi t).$$

Figure 3 displays the numerical solution by Green-CAS and exact solutions with fixed values of $k = 3$, $M = 4$, $\alpha = 1.85$, $\beta = 2$, and $\gamma = 0.35$. Likewise, in Figure 4, we present the graphical representation of the numerical and exact solutions with the same fixed values, except for $\gamma = 0.75$. Moreover, Figure 5 represents the error for $\alpha = 2$, $\beta = 2$, $\gamma = 0.25$, under various combinations of k and M, further validating the convergence of the proposed method.

Example 5.3 *[45] Consider the initial-boundary value fractional problem defined by*

$$\begin{aligned} \frac{\partial^\alpha u(x,t)}{\partial t^\alpha} &= \frac{\partial^2 u(x,t)}{\partial x^2} + \sin(\pi x), \\ &0 \le t \le 1,\ 0 \le x \le 1,\ \ 1 < \alpha \le 2, \\ &u(0,t) = 0,\ u(1,t) = 0,\ u(x,0) = 0, \\ &\left.\frac{\partial u(x,t)}{\partial t}\right|_{t=0} = 0. \end{aligned} \tag{43}$$

The analytic solution to the equation (43) can be expressed as $u(x,t) = \frac{1}{\pi^2}\left(1 - \sum_{k=0}^{\infty}\frac{(-\pi^2 t^\alpha)^k}{\Gamma(\alpha+1)}\right)\sin(\pi x)$. The numerical solutions are derived using the method described in Section 3.1.1. Both the exact and numerical solutions by Green-CAS for the parameters $\alpha = 1.75$, $k = 4$, and $M = 2$ are illustrated in tabular format in Table 4. A comparison is made between the numerical results obtained through our proposed method and the method discussed in [45]. The comparison, as shown in Table 4, reveals that our proposed method yields better results. Moreover, Table 5 displays the numerical confirmation of the convergence order, as outlined in the error analysis, for the variables k and M.

5.2 Nonlinear Fractional Problem

In this subsection, we focus on solving nonlinear FPDEs by combining the Picard iteration scheme with the Green-CAS and fast Green-CAS methods. To address nonlinear

Table 1. Comparing the present method with other techniques using absolute error for $\alpha = 1$, $k = 5$, and $M = 5$ for Example 5.1.

t	x	VIM and ADM [44]	S-LCM [43]	Green-CAS
0.25	0.3	1.54×10^{-5}	9.92×10^{-8}	8.42×10^{-8}
	0.6	6.16×10^{-5}	2.70×10^{-6}	2.93×10^{-8}
	0.9	1.38×10^{-4}	1.02×10^{-5}	5.82×10^{-8}
0.50	0.3	2.60×10^{-4}	5.56×10^{-7}	9.11×10^{-8}
	0.6	1.03×10^{-3}	4.87×10^{-6}	4.87×10^{-7}
	0.9	2.34×10^{-3}	1.30×10^{-5}	8.53×10^{-7}
0.75	0.3	1.39×10^{-3}	1.14×10^{-6}	1.06×10^{-6}
	0.6	5.56×10^{-3}	6.90×10^{-6}	1.75×10^{-6}
	0.9	1.25×10^{-2}	1.59×10^{-5}	2.49×10^{-6}

Table 2. Numerical order of convergence of Green-CAS method for M and k, in the context of Example 5.1.

	$M = 3$			$k = 3$	
k	L_2	Order	M	L_2	Order
2	1.64907×10^{-3}		4	4.00418×10^{-4}	
3	5.83670×10^{-4}	1.4984	5	2.96360×10^{-4}	1.3511
4	2.06415×10^{-4}	1.4996	6	2.30681×10^{-4}	1.2847
5	7.29837×10^{-5}	1.4999	7	1.86124×10^{-4}	1.2394
6	2.58041×10^{-5}	1.5000	8	1.54267×10^{-4}	1.2065
7	9.12316×10^{-6}	1.5000	9	1.30563×10^{-4}	1.1815

Table 3. Comparison of maximum absolute error and CPU time at different time steps for Example 5.1 at $\alpha = 0.73$.

Time steps	Space steps	Fast Green-CAS	CPU time(sec)	Green-CAS	CPU time(sec)
416	$k = 5,\ M = 5$	1.19804×10^{-4}	0.258	1.28874×10^{-4}	0.403
832		4.85058×10^{-5}	0.447	6.89939×10^{-5}	1.412
1664		1.90083×10^{-5}	0.747	3.65349×10^{-5}	9.747
3328		7.38037×10^{-6}	0.981	1.91559×10^{-5}	23.264

Table 4. Comparison of numerical results for $\alpha = 1.75$, $k = 4$, $M = 2$ for the Example 5.3.

t	x	Exact solutions	Method [45]	Green-CAS
0.2	0.25	0.0242284	0.0244444	0.0242273
	0.5	0.0342641	0.0323405	0.0342626
	0.75	0.0242284	0.0246124	0.0242273
0.5	0.25	0.0864843	0.0830947	0.0864560
	0.5	0.1223070	0.1167480	0.1222672
	0.75	0.0864843	0.0886781	0.0864560
0.8	0.25	0.1140370	0.1052860	0.1140223
	0.5	0.1612720	0.1490310	0.1612519
	0.75	0.1140370	0.1140710	0.1140223

https://doi.org/10.57647/mathsci.2025.1902.18

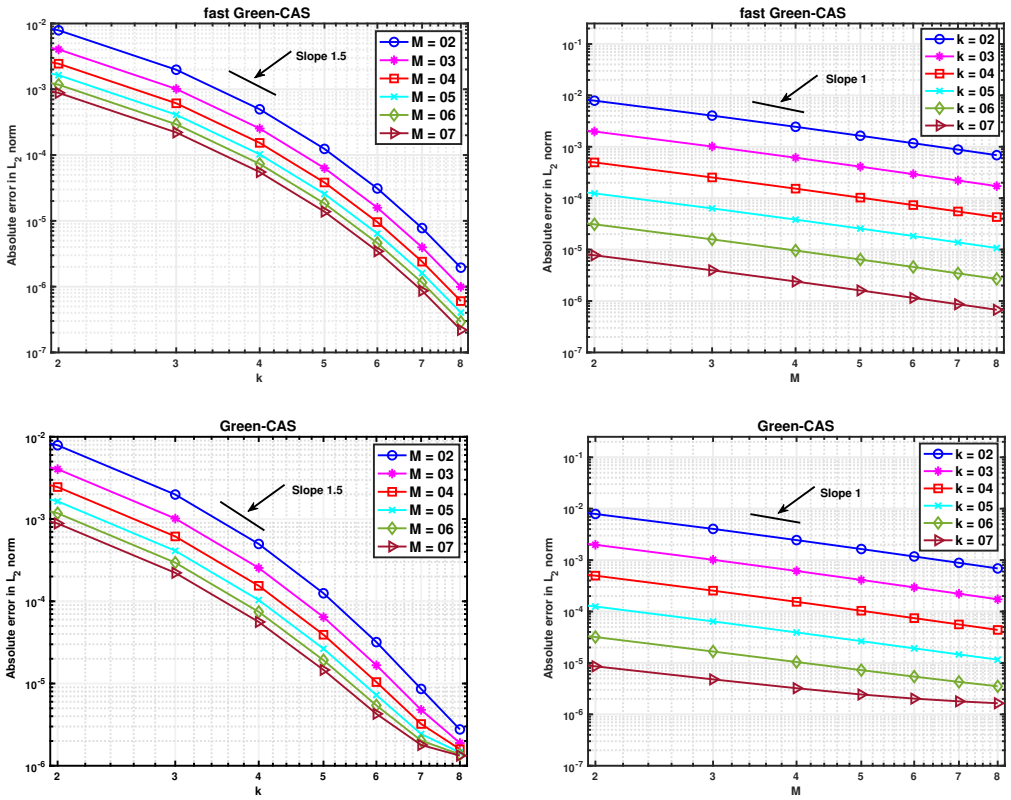

Figure 1. Absolute error in L_2 norm of fast Green-CAS and Green-CAS for $\alpha = 0.34$ at 832 time steps with different values of k and M in Example 5.1

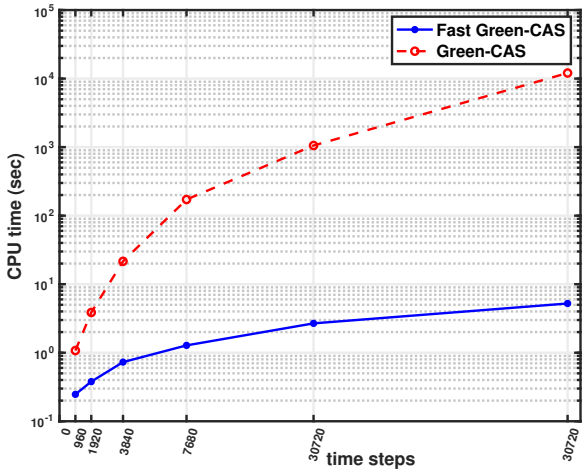

Figure 2. CPU time comparison between the fast Green-CAS and Green-CAS methods at different time steps, for fixed parameters $\alpha = 0.71$, $k = 4$, and $M = 5$ in Example 5.1.

FPDEs, we employ the Picard iterative method, which facilitates the linearization of nonlinear terms through successive approximations. The resulting linear problems are then efficiently solved using the Green-CAS or fast Green-CAS techniques described in Section 3. We consider the following nonlinear FPDE , along with its associated initial and boundary conditions

$$\begin{aligned} &\frac{\partial^{\alpha} u(x,t)}{\partial t^{\alpha}} + v(x)\frac{\partial^{\beta} u(x,t)}{\partial x^{\beta}} \\ &+w(x)u(x,t)\frac{\partial^{\gamma} u(x,t)}{\partial x^{\gamma}} + y(x)u^{p}(x,t) = f(x,t), \\ &\alpha,\beta \in (1,2],\ \gamma \in (0,1),\ \text{ and } p > 1, \end{aligned} \tag{44}$$

https://doi.org/10.57647/mathsci.2025.1902.18

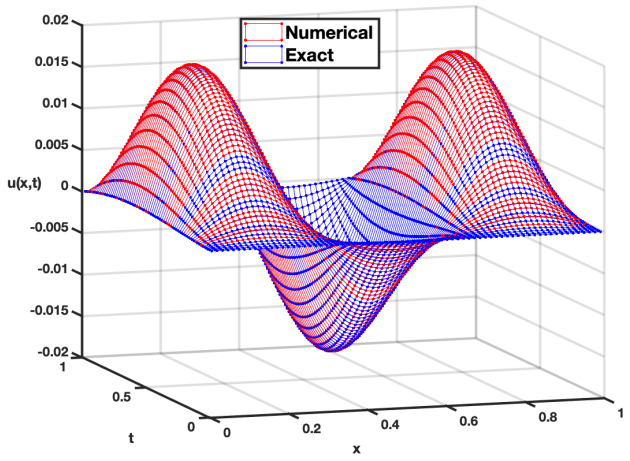

Figure 3. Exact and numerical solutions for Example 5.2 with $k = 3$, $M = 4$, $\alpha = 1.85$, $\beta = 2$, and $\gamma = 0.35$.

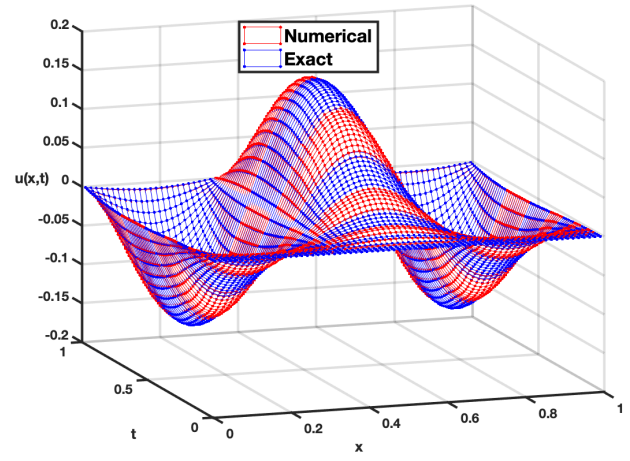

Figure 4. Exact and numerical solution for $k = 3$, $M = 4$, $\alpha = 1.85$, $\beta = 2$, and $\gamma = 0.75$ for Example 5.2.

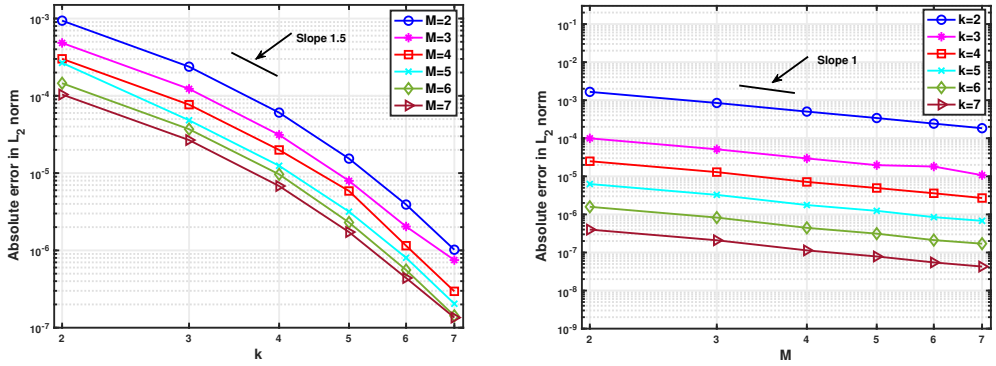

Figure 5. L_2 error between the exact and numerical solutions for Example 5.2 computed by Green-CAS, for different values of M and k.

$$u(a,t) = u_a(t), \quad u(b,t) = u_b(t),$$
$$(i) \quad u(x,c) = u_c(x), \quad u(x,d) = u_d(x)$$
$$or$$
$$(ii) \quad u(x,c) = u_c(x), \quad \frac{\partial u(x,t)}{\partial t}\bigg|_{t=c} = u_d(x),$$

Applying the Picard iteration method, as described in [46] to equation (44), yields the following iterative update formulation

$$\frac{\partial^\alpha u_{r+1}(x,t)}{\partial t^\alpha} + v(x)\frac{\partial^\beta u_{r+1}(x,t)}{\partial x^\beta} = U(x,t,u_r(x,t)\frac{\partial^\gamma u_r(x,t)}{\partial x^\gamma}), \qquad (45)$$

https://doi.org/10.57647/mathsci.2025.1902.18

Table 5. Numerical order of convergence of M and k, in the context of Example 5.3.

	$M=3$			$k=3$	
k	L_2	Order	M	L_2	Order
2	1.80559×10^{-4}		4	4.38666×10^{-5}	
3	6.39380×10^{-5}	1.4977	5	3.24680×10^{-5}	1.3511
4	2.26145×10^{-5}	1.4994	6	2.52729×10^{-5}	1.2847
5	7.99624×10^{-6}	1.4999	7	2.03915×10^{-5}	1.2394
6	2.82717×10^{-6}	1.5000	8	1.69015×10^{-5}	1.2065
7	9.99562×10^{-7}	1.5000	9	1.43046×10^{-5}	1.1815

subject to the corresponding initial and boundary conditions

$$u_{r+1}(a,t)=u_a(t),\quad u_{r+1}(b,t)=u_b(t),$$
$$(i)\quad u_{r+1}(x,c)=u_c(x),\quad u_{r+1}(x,d)=u_d(x)$$
$$or$$
$$(ii)\quad u_{r+1}(x,c)=u_c(x),\quad \left.\frac{\partial u_{r+1}(x,t)}{\partial t}\right|_{t=c}=u_d(x),$$

where $U(x,t,u_r(x,t)\frac{\partial^\gamma u_r(x,t)}{\partial x^\gamma})=w(x)u_r(x,t)\frac{\partial u_r(x,t)}{\partial x^\gamma}+y(x)u_r^p(x,t)+f(x,t)$. Subsequently, the updated linearized problem is solved using the proposed methods outlined in Section 3 to compute the approximate numerical solution.

Example 5.4 *Consider the generalized Burgers-Fisher equation along with the initial and boundary conditions*

$$\frac{\partial u(x,t)}{\partial t}-\frac{\partial^2 u(x,t)}{\partial x^2}+au(x,t)^\eta\frac{\partial u(x,t)}{\partial x}$$
$$+bu(x,t)\Big(u(x,t)^\eta-1\Big)=0,\ 0\le x\le 1,\ t\ge 0, \quad (46)$$

$$u(x,0)=\left(\tfrac{1}{2}-\tfrac{1}{2}\tanh\left(\tfrac{a\eta}{2(1+\eta)}x\right)\right)^\eta,$$
$$u(0,t)=\left(\tfrac{1}{2}-\tfrac{1}{2}\tanh\left(\tfrac{a\eta}{2(1+\eta)}\left[\left(-\tfrac{a^2+b(1+\eta^2)}{a(1+\eta)}\right)t\right]\right)\right)^\eta,$$
$$u(1,t)=\left(\tfrac{1}{2}-\tfrac{1}{2}\tanh\left(\tfrac{a\eta}{2(1+\eta)}\left[\left(1-\tfrac{a^2+b(1+\eta^2)}{a(1+\eta)}\right)t\right]\right)\right)^\eta.$$

The exact solution of the equation (46) is $u(x,t)=\left(\frac{1}{2}-\frac{1}{2}\tanh\left(\frac{a\eta}{2(1+\eta)}\left[\left(x-\frac{a^2+b(1+\eta^2)}{a(1+\eta)}\right)t\right]\right)\right)^\eta$. *The numerical solution to equation (46) is obtained using the Green-CAS technique in conjunction with the Picard iteration method. Table 6 and Table 7 present the absolute error comparisons between our proposed method and other established techniques. Table 6 reports the results for* $a=0.001$, $b=0.001$, $\eta=1$, *with* $r=4$, $k=3$, *and* $M=3$, *where our method is compared against the VIM and RDTM which are discussed in [47], as well as the CAS wavelet method from [48]. Table 7 further compares our results with the Adomian Decomposition Method (ADM) [49] and CAS wavelets [48] for the values of* $a=0.001$, $b=0.001$, $\eta=1$, $r=4$, $k=4$, *and* $M=3$. *These results demonstrate that the proposed method consistently yields superior accuracy and robustness in solving nonlinear FPDE, particularly when compared to traditional operational wavelet-based and decomposition techniques. This hybrid approach enables an efficient and accurate treatment of the nonlinear problem.*

Example 5.5 *Consider the time-fractional Burgers equation as presented in [50],*

$$\frac{\partial^\alpha u(x,t)}{\partial t^\alpha}-u(x,t)\frac{\partial u(x,t)}{\partial x}-v\frac{\partial^2 u(x,t)}{\partial x^2}$$
$$=f(x,t),\quad 0<\alpha\le 1. \quad (47)$$
$$u(0,t)=0,\quad u(1,t)=-t^{3/2},$$
$$u(x,0)=0.$$

The exact solution to equation (47) is given by $u(x,t)=t^{\frac{3}{2}}\sin(\frac{3\pi}{2}x)$, *which allows us to define the source term* $f(x,t)$ *as* $f(x,t)=\left[t^{\frac{3}{2}-\alpha}/\Gamma(\frac{5}{2}-\alpha)\right]\Gamma(\frac{5}{2})\sin(\frac{3\pi}{2}x)+\frac{3\pi}{2}t^3\sin(\frac{3\pi}{2}x)\cos(\frac{3\pi}{2}x)+\frac{9\pi^2}{4}t^{\frac{3}{2}}\sin(\frac{3\pi}{2}x)$. *Using this formulation, we compute numerical solutions using the proposed Green-CAS and fast Green-CAS techniques. Table 8 compares the* L_2 *and* L_∞ *error norms of our methods with those reported in [50], demonstrating that both the Green-CAS and fast Green-CAS yield significantly improved accuracy. Particularly, the fast Green-CAS method shows notably better results. In addition, Figure 6 illustrates the error between the exact and numerical solutions for* $\alpha=0.7$, *highlighting the sensitivity to variations in* k *and* M. *Specifically, the left subplot corresponds to fixed* $M=5$, *while the right subplot uses fixed* $k=5$. *Furthermore, CPU time comparisons between the Green-CAS and fast Green-CAS methods are displayed in Figure 7, highlighting the superior computational efficiency of the fast Green-CAS approach.*

6. Conclusion

In this study, we have advanced the Green-CAS wavelet method to effectively solve both linear and nonlinear FPDEs. To enhance computational efficiency, a fast Green-CAS method is introduced, specifically designed for time-fractional orders $\alpha\in(0,1)$, combining the strengths of both fast algorithms and the Green-CAS formulation. For nonlinear FPDEs, the Picard iteration technique is applied to linearize the original problem,

Table 6. Comparison of numerical results of the Example 5.4 at the values $a = .001$, $b = .001$, $\eta = 1$, $r = 4$, $k = 3$, and $M = 3$.

x	t	VIM [47]	RDTM [47]	CAS[48]	Green-CAS
0.01	0.02	2.5031102×10^{-3}	0.49994×10^{-5}	1.9435×10^{-7}	1.11617×10^{-8}
	0.04	2.5081138×10^{-3}	0.99994×10^{-5}	2.7604×10^{-7}	2.03356×10^{-8}
	0.06	2.5131170×10^{-3}	1.49994×10^{-5}	3.3814×10^{-7}	2.78715×10^{-8}
	0.08	2.5181206×10^{-3}	1.99994×10^{-5}	3.8724×10^{-7}	3.40581×10^{-8}
0.04	0.02	9.9961959×10^{-3}	0.49975×10^{-5}	7.1200×10^{-7}	4.03010×10^{-9}
	0.04	1.0001189×10^{-2}	0.99975×10^{-5}	1.0346×10^{-6}	7.36037×10^{-9}
	0.06	1.0006190×10^{-2}	1.49975×10^{-5}	1.2805×10^{-6}	1.03583×10^{-8}
	0.08	1.0011191×10^{-2}	1.99975×10^{-5}	1.4781×10^{-6}	1.32320×10^{-8}
0.08	0.02	1.9979433×10^{-2}	0.49950×10^{-5}	1.2555×10^{-6}	3.16961×10^{-9}
	0.04	1.9984423×10^{-2}	0.99950×10^{-5}	1.8928×10^{-6}	5.11237×10^{-9}
	0.06	1.9989425×10^{-2}	1.49950×10^{-5}	2.3807×10^{-6}	6.59666×10^{-9}
	0.08	1.9994415×10^{-2}	1.99950×10^{-5}	2.7727×10^{-6}	8.00618×10^{-9}

Table 7. Comparing numerical results for the Example 5.4 with the specified values of $a = 0.001$, $b = 0.001$, $\eta = 1$, $r = 4$, $k = 4$, and $M = 3$.

x	t	ADM [49]	CAS[48]	Green-CAS
0.1	0.005	9.68763×10^{-6}	5.70883×10^{-7}	1.84840×10^{-10}
	0.01	1.93752×10^{-5}	9.29559×10^{-7}	5.14744×10^{-10}
0.5	0.005	9.68691×10^{-6}	6.87261×10^{-7}	1.47340×10^{-10}
	0.01	1.93738×10^{-5}	1.31043×10^{-6}	2.90985×10^{-10}
0.9	0.005	9.68619×10^{-6}	5.71285×10^{-7}	1.30110×10^{-10}
	0.01	1.93724×10^{-5}	9.30207×10^{-7}	2.98346×10^{-10}

Table 8. Comparison of numerical results for Example 5.5 with $\alpha = 0.5$, $k = 4$, $M = 4$, and $r = 3$, evaluated at various time levels t.

	Method [50]		Green-CAS		fast Green-CAS	
t	L_2 norm [50]	L_∞ norm [50]	L_2 norm	L_∞ norm	L_2 norm	L_∞ norm
0.5	3.6×10^{-5}	2.1×10^{-4}	1.55431×10^{-5}	2.04153×10^{-5}	6.59210×10^{-6}	7.93684×10^{-6}
0.75	2.0663×10^{-5}	1.2×10^{-4}	1.60375×10^{-5}	2.27417×10^{-5}	4.89288×10^{-6}	6.31828×10^{-6}
1.0	1.3491×10^{-5}	1.1×10^{-4}	1.10440×10^{-5}	1.80474×10^{-5}	3.67528×10^{-6}	6.07079×10^{-6}

https://doi.org/10.57647/mathsci.2025.1902.18

allowing each iteration to be efficiently solved using the proposed techniques. A detailed convergence analysis was carried out, in which we established the theoretical error bound for the truncated solution under the Green-CAS wavelet framework, thereby verifying the stability and accuracy of the proposed method with respect to the key numerical parameters. However, a complete theoretical error analysis of the full Green-CAS and fast Green-CAS methods remains challenging and will be addressed in future work.

Comprehensive numerical experiments were conducted to verify the methods' performance. The results, displayed in both tables and figures, demonstrate that the Green-CAS method consistently outperforms the conventional CAS wavelet method in terms of accuracy. Notably, Table 6 and Table 7 highlight how the proposed method closely approximates the exact solutions for both linear and nonlinear problems. Furthermore, the fast Green-CAS method significantly reduces computational time while preserving or even improving numerical accuracy, particularly for larger time step sizes. This is clearly shown in Table 3 and Table 8, as well as Figure 2 and Figure 7. Beyond improved performance, the method is straightforward to implement and readily extendable to higher-dimensional problems, making it a practical and robust tool for solving complex FPDEs in various scientific and engineering applications.

CRediT authorship contribution statement

Muhammad Ismail: Writing – review & editing, Writing – original draft, Visualization, Validation, Software. **Bongsoo Jang:** Writing – review & editing, Validation, Conceptualization, Supervision, Resources, Funding acquisition, Formal analysis.

Acknowledgments

This work was supported by the National Research Foundation of Korea (NRF) grant funded by the Korean government (MSIT) (NRF-2021R1A2C1011817) and the BK21 Program(Next Generation Education Program for Mathematical Sciences, 4299990414089) funded by the Ministry of Education(MOE).

Authors contributions
All the authors have participated sufficiently in the intellectual content, conception and design of this work or the analysis and interpretation of the data (when applicable), as well as the writing of the manuscript.
Availability of data and materials
Data will be made available on request.
Conflict of interests
The author declare that they have no known competing financial interests or personal relationships that could have appeared to influence the work reported in this paper.

References

1. Lee S, Kim H, and Jang B. A novel numerical method for solving nonlinear fractional-order differential equations and its applications. Fractal and Fractional 2024; 8:65
2. Masti I and Sayevand K. On collocation-Galerkin method and fractional B-spline functions for a class of stochastic fractional integro-differential equations. Mathematics and Computers in Simulation 2024; 216:263–87
3. Sivalingam SM, Kumar P, Trinh H, and Govindaraj V. A novel L1-Predictor-Corrector method for the numerical solution of the generalized-Caputo type fractional differential equations. Mathematics and Computers in Simulation 2024; 220:462–80
4. Zhang X, Feng Y, Luo Z, and Liu J. A spatial sixth-order numerical scheme for solving fractional partial differential equation. Applied Mathematics Letters 2025; 159:109265
5. Ghoreyshi A, Abbaszadeh M, Zaky MA, and Dehghan M. Finite block method for nonlinear time-fractional partial integro-differential equations: stability, convergence, and numerical analysis. Applied Numerical Mathematics 2025; 214:82–103
6. Lee S, Lee J, Kim H, and Jang B. A fast and high-order numerical method for nonlinear fractional-order differential equations with non-singular kernel. Applied Numerical Mathematics 2021; 163:57–76
7. Tamboli VK and Tandel PV. Solution of the time-fractional generalized Burger–Fisher equation using the fractional reduced differential transform method. Journal of Ocean Engineering and Science 2022; 7:399–407
8. Chen H and Zhang H. New multiple soliton solutions to the general Burgers-Fisher equation and the Kuramoto-Sivashinsky equation. Chaos, Solitons & Fractals 2004; 19:71–6
9. Ödiz F, Tangolu G, Aghazadeh N, and Mohammadi A. An effective Legendre wavelet technique for the time-fractional Fisher equation. Computational Methods for Differential Equations 2025
10. Ahmadnezhad G, Aghazadeh N, and Rezapour S. Haar wavelet iteration method for solving time fractional Fisher's equation. Computational Methods for Differential Equations 2020; 8:505–22

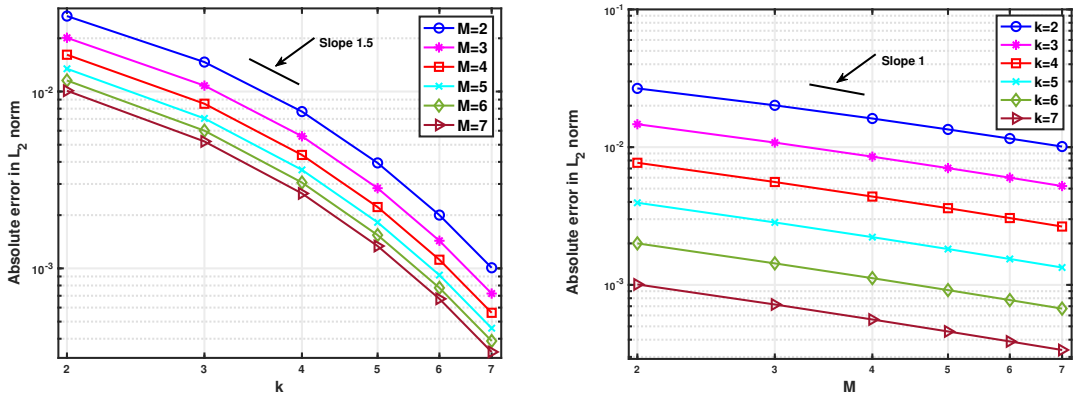

Figure 6. L_2 error norm for Example 5.5 computed using the Green-CAS method with $\alpha = 0.7$ and $r = 3$, for various values of M and k.

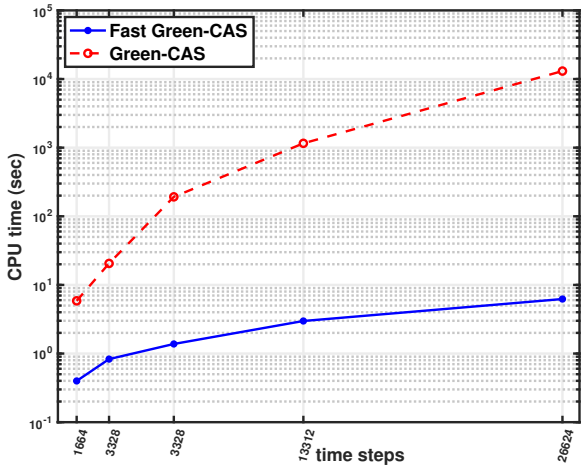

Figure 7. CPU time comparison between the fast Green-CAS and Green-CAS methods for $\alpha = 0.65$, $k = 5$, $M = 4$, and $r = 3$ in Example 5.5.

11. Mesgarani H, Esmaeelzade Aghdam Y, and Vafapisheh M. A numerical procedure for approximating time fractional nonlinear Burgers–Fisher models and its error analysis. AIP Advances 2023; 13:1–8
12. Aghazadeh N. A Chebyshev wavelet approach to the generalized time-fractional Burgers–Fisher equation. Computational Methods for Differential Equations 2025; 13:1135–47
13. Iagar RG and Sánchez A. Traveling wave solutions for the generalized Burgers–Fisher equation. arXiv preprint 2025. eprint: arXiv:2509.24909
14. Shallu S and Kukreja VK. Highly accurate collocation methodology for solving the generalized Burgers–Fisher's equation. Iranian Journal of Numerical Analysis and Optimization 2024; 14:736–61
15. Salih OM and Majeed AJ. Reliable iterative methods for solving 1D, 2D and 3D Fisher's equation. IIUM Engineering Journal 2021; 22:138–66
16. Al-Rozbayani AM and Al-Hayalie KA. Numerical Solution of Burgers–Fisher Equation in One-Dimensional Using Finite Differences Methods. Fluid Mechanics 2018; 4:20–6
17. Rashidi MM, Ganji DD, and Dinarvand S. Explicit analytical solutions of the generalized Burger and Burger–Fisher equations by homotopy perturbation method. Numerical Methods for Partial Differential Equations 2009; 25:409–17
18. Gurbuz B and Sezer M. Modified Laguerre Matrix Approach for Burgers–Fisher Type Nonlinear Equations. *Numerical Solutions of Realistic Nonlinear Phenomena*. Vol. 92. 2020 :1053–77
19. Singh A, Dahiya S, and Singh SP. A fourth-order B-spline collocation method for nonlinear Burgers–Fisher equation. Mathematical Sciences 2020; 14:75–85
20. Dahmen W, Kurdila A, and Oswald P. Multiscale Wavelet Methods for Partial Differential Equations. Academic Press, 1997
21. Abdi-Mazraeh S, Irandoust-Pakchin S, and Adel M. The construction of stochastic operational matrix via sparsity properties using B-spline wavelets to solve fractional stochastic integro-differential equations. International Journal of Dynamics and Control 2025; 13:1–14

22. Saeed U and Rehman M ur. A new scheme for the solution of the nonlinear Caputo–Hadamard fractional differential equations. Alexandria Engineering Journal 2024; 105:56–69
23. Ismail M, Rehman M ur, and Saeed U. Green–Haar method for fractional partial differential equations. Engineering Computations 2019; 37:1473–90
24. Shariati NM, Yaghouti M, and Alipanah A. On solving some stochastic delay differential equations by Daubechies wavelet. Journal of Statistical Computation and Simulation 2024; 94:1445–61
25. Khan H, Shah R, Arif M, and Bushnaq S. The Chebyshev Wavelet Method (CWM) for the Numerical Solution of Fractional HIV Infection of CD4+ T Cells Model. International Journal of Applied and Computational Mathematics 2020; 6:1–17
26. Irfan N and Siddiqi AH. An application of wavelet technique in numerical evaluation of Hankel transforms. International Journal of Nonlinear Sciences and Numerical Simulation 2015; 16:293–9
27. Irfan N and Siddiqi AH. A wavelet algorithm for Fourier–Bessel transform arising in optics. International Journal of Engineering Mathematics 2015; 2015:Article ID 789675
28. Irfan N, Singh VK, and Kapoor S. Review of some Askey-scheme of hypergeometric orthogonal polynomials. International Transactions in Applied Sciences 2011; 2:459–74
29. Irfan N, Alam M, and Alam K. A systematic analysis of a novel Hankel transform wavelet framework and its complexity implications. Journal of Computational Analysis and Applications 2024; 33
30. Yousefi S and Banifatemi A. Numerical solution of Fredholm integral equations by using CAS wavelets. Applied Mathematics and Computation 2006; 183:458–63
31. Taher A, Ibrahim S, and Marwan A. Optimal Control Systems by Time-Dependent Coefficients Using CAS Wavelets. Journal of Applied Mathematics 2009; 2009:1–10. DOI: 10.1155/2009/636271
32. Barzkar A, Assari P, and Mehrpouya MA. Application of the CAS wavelet in solving Fredholm–Hammerstein integral equations of the second kind with error analysis. World Applied Sciences Journal 2012; 18:1695–704
33. Yi M, Sun K, Huang J, and Wang L. Numerical solutions of fractional integro-differential equations of Bratu type by using CAS wavelets. Journal of Applied Mathematics 2013; 2013:1–7
34. Ismail M, Saeed U, Alzabut J, and Rehman M. Approximate Solutions for Fractional Boundary Value Problems via Green–CAS Wavelet Method. Mathematics 2019; 7:1164
35. Diethelm K. The Analysis of Fractional Differential Equations. Lecture Notes in Mathematics. Springer, 2010
36. Podlubny I. Fractional Differential Equations. San Diego: Academic Press, 1999
37. Benedetto JJ and Frazier WM. Wavelets: Mathematics and Applications. CRC Press, Taylor & Francis Group, 2021
38. Kilicman A and Al Zhour ZAA. Kronecker operational matrices for fractional calculus and some applications. Applied Mathematics and Computation 2017; 187:250–65
39. Li Y and Sun N. Numerical solution of fractional differential equations using the generalized block pulse operational matrix. Computers and Mathematics with Applications 2011; 62:1046–54
40. Miller KS and Ross B. An Introduction to the Fractional Calculus and Fractional Differential Equations. New York: John Wiley and Sons Inc., 1993
41. Jiang S, Zhang J, Zhang Q, and Zhang Z. Fast evaluation of the Caputo fractional derivative and its applications to fractional diffusion equations. Communications in Computational Physics 2017; 21:650–78
42. Majak J, Shvartsman BS, Kirs M, Pohlak M, and Herranen H. Convergence theorem for the Haar wavelet based discretization method. Composite Structures 2015; 126:227–32
43. Saadatmandi A, Dehghan M, and Azizi MR. The Sinc–Legendre collocation method for a class of fractional convection–diffusion equations with variable coefficients. Communications in Nonlinear Science and Numerical Simulation 2012; 17:4125–36
44. Molliq Y, Noorani MSM, and Hashim I. Variational iteration method for fractional heat- and wave-like equations. Nonlinear Analysis: Real World Applications 2009; 10:1854–69
45. Ebadi MA and Hashemizadeh E. A new approach based on the Zernike radial polynomials for numerical solution of the fractional diffusion-wave and fractional Klein–Gordon equations. Physica Scripta 2018; 93:125202
46. Bellman RE and Kalaba RE. Quasilinearization and nonlinear boundary-value problems. New York: American Elsevier Publishing Company, 1965
47. Kocacoban D, Koc AB, Kurnaz A, and Keskin Y. A better approximation to the solution of Burger–Fisher equation. *Proceedings of the World Congress on Engineering*. Vol. I. 2011
48. Saeed U and Gilani K. CAS wavelet quasilinearization technique for the generalized Burger–Fisher equation. Mathematical Sciences 2018; 12:61–9

49. Ismail HN, Raslan K, and Rabboh AAA. Adomian decomposition method for Burger's–Huxley and Burger's–Fisher equations. Applied Mathematics and Computation 2004; 159:291–301

50. Majeed A, Kamran M, Iqbal MK, and Baleanu D. Solving time fractional Burgers' and Fisher's equations using cubic B-spline approximation method. Advances in Difference Equations 2020; 2020:175

https://doi.org/10.57647/mathsci.2025.1902.18